Title: Size and shape regional differentiation during the development of the spine in the nine-banded armadillo (*Dasypus novemcinctus*).

Jillian D. Oliver[1], Katrina E. Jones[1], Stephanie E. Pierce[1]*, and Lionel Hautier[2]*

[1]Museum of Comparative Zoology and Department of Organismic and Evolutionary Biology, Harvard University, Cambridge, MA, 02138, USA

[2]Institut des Sciences de l'Evolution, UMR 5554, CNRS, IRD, EPHE, Université de Montpellier, Montpellier, France

*Corresponding authors: lionel.hautier@umontpellier.fr and spierce@oeb.harvard.edu

Abstract

Xenarthrans (armadillos, anteaters, sloths and their extinct relatives) are unique among mammals in displaying a distinctive specialization of the posterior trunk vertebrae - supernumerary vertebral xenarthrous articulations. This study seeks to understand how xenarthry develops through ontogeny and if its development impacts regionalisation patterns (thoracic vs lumbar). Using 3D geometric morphometrics on the neural arches of vertebrae, we explore phenotypic, allometric, and disparity patterns of the different axial morphotypes during ontogeny of nine-banded armadillos. Shape-based regionalisation analyses showed that adult thoracolumbar column is divided into three regions according to the presence or absence of ribs and the presence or absence of xenarthrous articulations. A three-region-division was retrieved in almost all specimens through development, although younger stages (e.g. embryos, neonates) have more region boundary variability. In size-based regionalisation analyses, thoracolumbar vertebrae are separated into two regions according to the presence or absence of xenarthry. We show that xenarthrous thoracic vertebrae grow at a slower rate, while anterior thoracics and lumbar grow at a faster rate relatively, with rates decreasing anteroposterioly in the former and increasing anteroposterioly in the latter. We propose that different proportions between vertebrae and vertebral regions might result from differences in growth pattern and timing of ossification, which might in turn correlate with expression patterns of *Hox* genes.

INTRODUCTION

The vertebral column and its associated epaxial musculature function to maintain posture, propel the body, and act as an axis upon which limbs can move (e.g. Koob and Long, 2000). Across vertebrate lineages, the diversity of vertebral morphologies and patterning schemes reflects the breadth of modes of locomotion (e.g. Rockwell et al., 1938; Hebrank et al., 1990; Gal, 1993; Gál, 1993; Long et al., 1997; Boszczyk et al., 2001; Buchholtz, 2001; Pierce et al., 2011; Schilling, 2011). Vertebral patterning, i.e. the regionalisation of vertebrae into distinct functional units, is implicated in the ecological and locomotor niches occupied by vertebrates (e.g.Rockwell et al., 1938; Buchholtz, 2007; Jones and German, 2014; Jones et al., 2018a, 2018b, 2020). In mammals, the prominence of asymmetric running gaits is facilitated by the division of the dorsal vertebrae into ribbed thoracic and rib-less lumbar regions. The thoracic region is further divided according to the diaphragmatic vertebra, which coincides with a shift in zygapophyseal morphology and thus intervertebral articulation.

Among mammals, xenarthrans (armadillos, anteaters, sloths and their extinct relatives) represent a special case. In this group, the distinction between pre-diaphragmatic and post-diaphragmatic vertebrae is further defined by the presence of supernumerary vertebral articulations: the xenarthrous articulations or xenarthrales. These articulations correspond to accessory intervertebral articulations formed between the anapophysis of a vertebra and the metapophysis of the vertebra immediately caudal to it, which span the posterior thoracic and lumbar regions and generally overlap with the post-diaphragmatic region (Gaudin, 1999; Oliver et al., 2016). Xenarthry is found in all modern and extinct xenarthrans with the exceptions of extant sloths and glyptodonts (Gaudin, 1999). It has been linked to evolution toward a fossorial lifestyle, the suggested ancestral locomotor mode of the lineage (Simpson, 1931; Frechkop,

1949; Jenkins, 1970; Gaudin and Biewener, 1992; Vizcaino and Milne, 2002; Nyakatura and Fischer, 2011; Emerling and Springer, 2015; Oliver et al., 2016; Olson et al., 2016). Recently, Oliver et al. (2016) demonstrated that xenarthrous vertebrae constitute a passively stiff region within the armadillo vertebral column, a functional attribute hypothesized to facilitate fossoriality by bracing the body, thereby providing leverage to the limbs during digging (Frechkop, 1949; Jenkins, 1970; Gaudin and Biewener, 1992).

Xenarthrous articular morphology has been well described across both fossil and extant xenarthran species (Gaudin, 1999), but transitional forms are unknown in the fossil record (MacPhee, 1994). On the other hand, developmental data has offered unique insights into the phenotypic trajectory of xenarthrous vertebrae through xenarthran evolutionary history (Hautier et al., 2018), and invalidated the hypothesis that xenarthrous articulations represent a type of sacralization of the posterior thoracic and lumbar regions of xenarthran vertebral columns. However, the impact of xenarthrales on regionalisation patterns of the vertebral columns has never been thoroughly explored. Here we ask how xenarthry has impacted mammalian regionalisation, and examine its developmental origins, using *Dasypus novemcinctus*, the nine-banded armadillo. We employ X-ray microtomography (X-ray μCT) and three-dimensional geometric morphometrics to describe vertebral shape at different developmental stages. We use this data to explore phenotypic, allometric, and disparity patterns of vertebrae through development, and characterize vertebral regions of the xenarthran spine and how they develop. As vertebrae acquire diverging complex morphologies associated with specialized features through development (Johnson and O'Higgins, 1994), we expect disparity and regionalisation to increase during ontogeny.

MATERIALS & METHODS

Material - μCT scans of six *Dasypus spp*. embryos, four neonates, two juveniles, and three adults were examined (Table 1). Scans were segmented using either Avizo version 7.1 or Mimics Materialise software version 17.0. Specimens covered an age range spanning the point at which all thoracolumbar vertebrae are ossified, through to adulthood, allowing us to examine the entire span of ossified vertebral development. While absolute ages of specimens were unknown, relative ages were assessed based on degree of vertebral ossification, and developmental stages were obtained from museum records. All individuals analysed were identified as *D. novemcinctus*, with the exception of ZMB 7b, whose species designation is unknown. All specimens from the Smithsonian Museum of Natural History (USNM) and the Museum of Comparative Zoology (MCZ) were μCT-scanned on a SkyScan 1173 at the Museum of Comparative Zoology, Harvard University, and reconstructed with NRecon version 1.6.6.0 (MCZ scans were also included in Oliver et al., 2016). All other scans were taken prior to the commencement of this study (Hautier et al., 2010, 2011).

Geometric morphometrics - All specimens have ten thoracic vertebrae (T1-10) and five lumbar vertebrae (L1-5), with the exception of UM-M1508, which has four lumbar vertebrae. In order to quantify the changes of shape across development, sixteen homologous landmarks were assigned to the left neural arch of all thoracolumbar vertebrae in each specimen with *MorphoDig* (Lebrun, 2014; Fig. 1). Analyses were restricted to neural arches as centra were absent in some cases or too poorly mineralized to enable performing morphometric comparisons. Landmarks were chosen to adequately capture the shape and the morphological transformations of the vertebrae (Table 2). Since most of the specimens analysed were developmentally immature, landmarks

were assigned predominantly to structures identifiable in all vertebrae at all stages. However, the two structures associated with xenarthry, the metapophysis and anapophysis, are for the most part present only in vertebrae participating in xenarthrous articulations. Additionally, the anapophysis is only visible postnatally. To address the absence of these structures in a large subset of vertebrae sampled, we followed Klingenberg (2008), who suggested that in order to measure morphological novelty, landmarks should be assigned to the structure of interest when present, and to the position from which it would emerge when absent. This protocol has since been adapted for vertebral column, facilitating the quantification of morphologies present only in a subset of vertebrae under study (Head and Polly, 2015; Oliver et al., 2016; Jones et al., 2018a). We then performed geometric morphometric analyses on vertebral morphology to measure vertebral shape variance using the R package *geomorph* (Adams et al., 2020). All configurations (sets of landmarks) were superimposed using the Procrustes method of generalized least squares superimposition (GLS scaled, translated, and rotated configurations so that the intralandmark distances were minimized) and shape variability of the vertebrae was analysed by principal components analysis (PCA).

Regionalisation analysis - In order to examine the establishment of morphological regions during ossification of the vertebral column, we compared regionalisation patterns across developmental stages using the R package *Regions* (Jones et al., 2018b). We established region number and boundaries using a multivariate segmented regression approach that models regions as gradients, and maximum likelihood to select the optimal number of segments (Head and Polly 2015). For each specimen, every combination of regions was modelled iteratively, up to a maximum of six, based on either the Centroid Size (size analysis) or the top five PCs (shape analysis). The Akaike

Information Criterion, corrected for small sample sizes, was used to determine the optimal regionalisation model (Jones et al., 2018b). The craniocaudal location of region breaks for each specimen was determined based on the position of the segmented regression boundaries in the best fit model. However, the curvilinear relationship between vertebral position and morphology introduces some error into boundary estimation, and thus boundary positions were considered accurate to within one vertebra (i.e., vertebral position +/- one).

Phenotypic trajectory analyses – To determine the changes in regional gradient occurring through development, we used phenotypic trajectory analysis (PTA) (Adams and Collyer, 2009; Collyer and Adams, 2013). PTA enabled us to examine ontogenetic trajectories from two perspectives: across osteological development, as well as the morphological relationships between vertebrae within age groups. In both cases, phenotypic trajectories were drawn in a morphospace determined by the first two PC axes. In the across-column PTA, paths were drawn between region averages (i.e. anterior and xenarthrous thoracics, and lumbars) within each age group (embryo, neonate, juvenile, adult), indicating the amount of morphospace occupied by columns of different ages. In the PTA of ontogenetic trajectories, paths were drawn between regional averages of each age group, highlighting the diverging morphology of the recognized vertebral regions through development. Length, direction, and shape of trajectories were statistically compared pairwise in both analyses. The *geomorph* function trajectory.analysis (RRPP package) was used for both PTA's (Adams et al., 2020).

Integration and disparity analyses - To understand the relative evolvability of different regions we conducted integration and disparity analyses. Integration values of vertebrae across the

column in every specimen were estimated as the standard deviation of the PCA eigenvalues accounting for 95% of shape variation (Young and Badyaev, 2006; Gómez-Robles and Polly, 2012). Greater dispersion of eigenvalues indicates stronger integration because it suggests more of the total variance is concentrated on just a few axes of variation. Following Gomez-Robles and Polly (2012), eigenvalues were standardized by total shape variance. This value provides a relative indication of the degree of morphological covariation between vertebrae in a single specimen, allowing us to assess the degree to which the vertebrae behave as a morphological unit. Conversely, values of disparity indicate the level of morphological diversity within the column, or within defined regions. These values allow us to assess the changes in morphological variability across developmental history. Disparity analyses were conducted using the *geomorph* function morphol.disparity, which uses Procrustes variation of a set of landmarks to measure pairwise morphological variance (Adams et al., 2020). Whole column disparity was calculated in each specimen, and regional (anterior thoracic, xenarthrous thoracic, lumbar) disparities were calculated in each age group (embryo, neonate, juvenile, adult). The assigned regions are in accordance with the adult regionalisation scheme predicted by the regionalisation analysis of centroid shape.

Vertebral differential growth – To determine vertebral growth rates, we compared the centroid size of each vertebra to size of the thoracolumbar region, estimated by the sum of the centroid sizes of all of its constituting vertebrae (i.e anterior thoracics, xenarthrous thoracics, and lumbars). First, we estimated the proportion of each vertebra, as compared to size of the thoracolumbar region, during the four defined developmental stages (i.e embryos, neonates, juveniles, and adults). We then performed multiple linear regressions of the centroid size of a

vertebral locus against the size of the thoracolumbar region for all individuals of the ontogenetic series, and used the slope as an estimator of growth for each vertebra (Anderson and Secor, 2016).

RESULTS

Vertebral regionalisation - Regionalisation analyses were performed using centroid size and shape on thoracic and lumbar vertebrae from every specimen in order to determine the optimal number of regions in the vertebral columns across development. Shape-based regionalisation analysis revealed that thoracolumbar vertebrae were most often divided into three regions across all stages of development (Fig. 2A; Table 3). The vertebrae were divided into only two regions in two embryos (specimens B and F), and into four regions in one neonate (specimen G). In the specimens in which the vertebrae were divided into three regions, the first break point ranged from T3-T6 (Table 3), which was situated at or anterior to the diaphragmatic vertebra, T7. The second breakpoint ranged from T7-T10 (Table 3), at or anterior to the thoracic-lumbar transition. In specimens B and F, the breakpoint between the two regions was T6 (Table 3). In specimen G, in which four regions were uncovered, the first two thoracic vertebrae formed their own region (Table 3). The three adults studied were found to have the same pattern of regionalisation, with breakpoints at T6 and T10 (Table 3), distinguishing a pre-diaphragmatic, pre-xenarthrous thoracic region (T1-6), a post-diaphragmatic, post-xenarthrous thoracic region (T7-T10), and a lumbar region (L1-5). Adults consistently display higher values of Akaike weights than the juveniles, which indicate a better estimation of their best model.

Size-based regionalisation analysis settled on two regions for all specimens, with the exception of specimen D, in which the first two thoracic vertebrae formed their own region (Fig.

2B; Table 3). In specimens with two regions, the breakpoint ranged from T4-T7, with T6 being the most common (Table 3). Size-based regionalisation therefore roughly distinguished a pre-diaphragmatic, pre-xenarthrous region, and a post-diaphragmatic, post-xenarthrous region, and does not differentiate between thoracic and lumbar vertebrae. In most cases, the location of the breakpoint was different between shape- and size-based regionalisation analyses, although it usually differs by only one vertebral position. No difference was observed in the values of Akaike weights between juveniles and adults.

Phenotypic trajectories – The PCA performed on all individual vertebrae (Fig. 3A) revealed that they present very similar morphology early in development. Developmental stages spread along PC1, with embryos and neonates occupying negative values and juveniles and adults the positive values. In contrast, vertebral regions spread along PC2: xenarthrous thoracics and lumbars are PC2 positive, and anterior thoracics are PC2 negative (Fig. 3A). Through ontogeny, we observed an increase in the amount of morphospace occupied by vertebrae, primarily along the second principal component (Fig. 3A). While embryonic vertebrae are not readily distinguishable from each other, xenarthrous thoracic and lumbar vertebrae take up gradually more morphospace through adulthood, allowing us to visualize the transition between vertebrae along the column along PC2 (Fig. 3A). In contrast, anterior thoracics seem to individualize early during development and occupy a distinct part of the morphospace, including in embryos in which they still diverge from other regions of the morphospace. Phenotypic trajectory analyses (PTAs; Fig. 3B and C) enabled us to examine in more detail this change in morphospace occupation across development. The first PTA traced trajectories between vertebral regions (anterior thoracics, xenarthrous thoracics, and lumbars) in the four stages of development (Fig. 3B). The four

developmental trajectories demonstrate a significant difference in size, as well as in direction except between juveniles and adults (Table 4). In contrast, they show no significant differences in shape (Table 4), the difference being almost significant between embryos and adults. The second PTA defined trajectories within regions across developmental stages and demonstrates the diverging morphological paths taken by the three regions through development (Fig. 3C). Xenarthrous thoracic and lumbar vertebrae display very similar trajectories at the beginning of the ontogenetic sequence, then gradually spread out to occupy distinct morphospaces in adulthood (PC1 positive). The three regional trajectories are significantly different from each other in direction (Table 5), but show no significant difference in shape. Anterior thoracics show significant differences in size trajectories with both xenarthrous thoracics and lumbars, which in turn do not significantly differ from each other (Table 5).

Vertebral disparity and integration – The whole-column disparity and integration were calculated for every specimen (Fig. 4A), and regional disparity was then calculated across developmental stages (Fig. 4B). Whole-column integration gradually increased through embryonic development, and rapidly increased in post-natal development (Fig. 4A). Whole-column disparity initially decreased from the embryo stage to the neonate stage, and then increased again in juveniles and adults (Fig. 4A), indicating that early development is characterized by a stage of relatively high morphological variability in vertebrae, while morphologies appear to converge in the neonatal stage. As with integration, disparity rapidly increased postnatally to reach a peak in adulthood.

Examining with-in regional disparity across stages of development allowed us to further dissect the disparity data (Fig. 4B). In all three regions, as defined by regionalisation analyses,

disparity significantly increased across development. The high disparity observed in adult vertebral columns was primarily localized to anterior thoracic (Ta) and lumbar (L) regions, which were significantly more disparate than they were in the three earlier stages of development (Table 6). A more modest increase in disparity is observed in the xenarthrous thoracic (Tx) region in adulthood, which was significantly different only from embryo and neonate disparities (Table 6). Embryo and neonate disparities were not significantly different from each other in any of the three regions (Table 6), despite a clear drop in disparity from the embryo to neonate stage in the anterior thoracic region (Fig. 4B). This decrease mimics that seen in whole-column disparity values, indicating that this pre- and neonatal drop in disparity is likely localized to the anterior thoracic region.

Regional axial growth – Vertebral proportions are very similar between ontogenetic stages (Fig. 5A), but two trends are noticeable: the mid-trunk region becomes relatively shorter, while most growth seems to occur toward the anterior and posterior extremes of the thoracolumbar region. The slope of the linear regressions of the centroid size of each vertebra against the size of the whole thoracolumbar region enabled us to estimate the growth patterns for each vertebra (Fig. 5B). Growth rates steadily decrease from the first thoracic vertebra to the first xenarthrous thoracic vertebra, to increase again up to the fourth lumbar vertebra, the last lumbar showing a slower rate than the vertebra just anterior to it. In sum, xenarthrous thoracic vertebrae seem to grow at a slower rate, while anterior thoracics and lumbar grow at a faster rate relatively (Fig. 5B). The rate decreases anteroposterioly in anterior thoracics, but increases anteroposterioly in lumbars.

DISCUSSION

The development of vertebrae proceeds from three ossification centres, the left and right vertebral arches and the centrum body. Two periods of vertebral growth were recognized during the development of the mouse vertebra (Bateman, 1954). The first phase corresponds to the fusion of the three ossification centres. The second phase consists of 'external accretion' at the level of the vertebral arch, which grows outwards and upwards, coupled with 'internal erosion' at the level of the neural canal (Bateman, 1954). On the centrum, endochondral ossification occurs at the epiphyses, and is mainly responsible for length increases. On the neural arches, periosteal ossification occurs at vertebral processes and is responsible for increases in height via appositional growth (Cubo et al., 2002; Valverde et al., 2010). By comparing vertebral development in different mouse strains, Johnson and O'Higgins, (1994) suggested that early-developing features tend to show a more conserved growth pattern. They hypothesized that features showing the greatest specialization should complete their development later rather than earlier. This was confirmed by descriptive developmental data in *Dasypus*, with basic shared features of the vertebrae ossifying earlier than the more specialized features (Hautier et al., 2018). In fact, the ossification of anapophyses and the differentiation in metapophysis and zygapophysis shape start quite late, at the neonate stage (Hautier et al., 2018). Compared to adults, embryos and juveniles display more homogeneous vertebral columns with little observable regional differentiation. These qualitative observations were confirmed here by our quantitative analyses, which enabled us to demonstrate that vertebral differentiation patterns might be more dynamic than previously conceived when looking at the full developmental sequence rather than adult morphology alone.

Regionalisation developmental dynamics - Qualitative examination of the adult *Dasypus* thoracolumbar region reveals that it is a morphologically complex series, and that intervertebral anatomical transitions are gradual (Hautier et al., 2018). Based on preliminary works on regionalisation (e.g. Head and Polly, 2015; Randau and Goswami, 2017a; Jones et al., 2018b), we expected the thoracolumbar vertebrae to be divided into three regions according to the diaphragmatic vertebra and the thoracic/lumbar transition. As *Dasypus* develops into its adult form, its thoracolumbar vertebral series becomes more consistently regionalised, as expected, and xenarthrous vertebrae adopt their unique morphology. In most embryos and pre-adults, the semi-xenarthrous vertebra (T6) is grouped with posterior thoracic vertebrae, suggesting that its shape is predominantly defined by its posterior xenarthrous articulation. This may also be a product of either the later ossification of the mid-thoracic vertebrae as compared to the anterior thoracics and lumbars (Hautier et al., 2010 and Fig. 6), or of the reduction of xenarthrous processes in a posterior-to-anterior direction, from L5-T7, in the adult. As the development of the vertebral column proceeds, the xenarthrous characteristics of T7, and of the succeeding vertebrae, become more pronounced, and T7-T10 consistently group in xenarthrous thoracics.

Unlike the consistent boundaries of the adult specimens, regional transitions in foetuses and stillborn appeared more variable. Such inconsistency likely results from imprecisions in boundary placement resulting from more subtle or more gradational transitions between regions. The approach applied here models the vertebral column as a segmented regression composed of a series of linear relationships. This model provides a better approximation in the adult specimens where the regions are clearly defined. Whereas, more curvilinear patterns in younger specimens make determining regional patterns more challenging. However, in shape-based regionalisation analyses, a three-region-division was obtained in almost all specimens (i.e. 12 out

of the 15 specimens). The main exceptions are two embryos in which only two regions were recognized, with a break point located at the diaphragmatic vertebra, and one embryo with four regions, in which the first two anterior thoracic vertebrae form their own region. This result suggests that axial shape regionalisation is conserved during development despite drastic changes in vertebral morphology. The distinction between non-xenarthrous and xenarthrous vertebrae rapidly becomes more discrete, as exemplified in the two embryos for which the thoracolumbar vertebrae are divided into two groups (Fig. 3B). Such results indicate that differentiation of vertebral regions in the xenarthran column is not directly coincident with the ontogenetic development of the specialized xenarthous joints, which only start to ossify at the neonate stage (Hautier et al., 2018), but instead occurs very early on during development when the shape of vertebrae remains quite simple. Most importantly, this two-region model likely reflects a subtler distinction between thoracics and lumbars than between non-xenarthrous and xenarthrous vertebrae. This was confirmed by the PTA results, with xenarthrous thoracic and lumbar vertebrae displaying more similar trajectories.

As is often the case in morphological evolution, allometry is likely to explain a substantial portion of the morphological differentiation of the spine, as size increases need to be adjusted by structural adaptation to static loading (Randau et al., 2016; Jones et al., 2018a). Our developmental data confirmed this in showing the significant influence of size on the regionalisation of the axial skeleton. In size-based regionalisation, two main regions can be recognized through development (Fig. 2B), with the break point located around the diaphragmatic vertebra. In one young embryo, however, the first two thoracic vertebrae form their own group again. This might be attributed to the fact that these two neural arches ossify earlier than the more caudal vertebrae (Hautier et al., 2010; Fig. 6), and are thus larger to a

variable extent. Apart from a few specimens, the diaphragmatic vertebra was consistently attributed to the posterior region whereas T6 inconsistently fits either of these two primary regions, probably as it displays transitional morphological characters reflective of both xenarthrous and non-xenarthrous vertebrae. Although intuitive, this size-based pattern cannot be attributed entirely to the presence of large metapophyses in xenarthrous vertebrae, because such protrusions are not developed until late during development. The metapophyses can only be identified in the youngest embryos as a small rounded bump, but become more and more distinguishable through development on the lumbar series, the xenarthrous thoracics following the same trajectory later during development (Hautier et al., 2018). Interestingly, the retrieved two-region model based on size, and on shape (specimen B and F, Fig. 2A) to a lesser extent, does not take into account the anatomically and functionally relevant distinction between the rib-bearing thoracic vertebrae and rib-less lumbar vertebrae. Such division might instead be linked to the development of the sternum, since postdiaphragmatic thoracics are the origin for the floating ribs in mammals, which are not connected to the former. Consequently, the distinction between anterior and xenarthrous thoracic regions might relate more to ribs than vertebrae themselves, and be reflective of their different function.

The mammalian vertebral column is commonly organized into cervical, thoracic, lumbar, sacral, and caudal regions according to a common *Hox* expression scheme, and to the functional relevance of each region (Burke et al., 1995; Wellik, 2007). The thoracolumbar regionalisation scheme described here in *Dasypus* reaches beyond what is typically suggested for mammals, with the thoracic region being divided into two morphological and possibly functional segments, the most posterior of which is identified both by articulation with ribs, and by the presence of xenarthrae. In terms of morphology alone, subdivision of thoracic vertebrae into two regions was

recently proposed for *M. musculus* and a variety of other amniotes (Head and Polly, 2015; Jones et al., 2018b), although the placement of the subdivision was taxon-specific and appears to correlate with the *Hox* code. Rather than a novel trait unique to xenarthrans, the additional regionalisation found in *Dasypus* may then constitute a shared feature of all mammals, and perhaps amniotes, and could be considered as an exaptation of an existing region to pattern a new type of morphology. Indeed, the morphological boundary between non-xenarthrous and xenarthrous vertebrae in *Dasypus* appears to roughly align with the *Hox*-expression boundaries established in *M. musculus* (Fig. 6; Wellik, 2007), suggesting that xenarthrous articulations might have evolved within the prescribed *Hox* boundaries common to all amniotes. This may also apply to other mammalian groups displaying specialized vertebral features, such as the highly modified thoracolumbar spine of hero shrews (Smith and Angielczyk, 2020). We showed that this distinction between anterior and posterior thoracics might be largely influenced by allometry, so that growth pattern may constitute a key feature underlying regionalisation differences.

Ontogenetic disparity and integration – As vertebrae acquire diverging complex morphologies associated with specialized features through development, disparity was expected to increase during ontogeny. Our results confirm this expectation with whole-column disparity increasing through development and vertebrae occupying more morphospace (Fig. 3). From neonates onward, however, all three regions display an increase in disparity, concurrent with the differentiation of more specialized structures (metapophysis, anapophysis, and zygapophysis). Following early embryonic development, the three vertebral regions occupy different parts of the morphospace and follow divergent paths through development, which is reflective of their

different functions (Oliver et al., 2016). This pattern seems to be already well established in juveniles and to a lesser extent in neonates (Fig. 3).

The drop in disparity that occurs from embryos to neonates was more unexpected, and is not reflected in the PT analyses. This developmental pattern of disparity can, however, find explanation in the peculiar ossification sequence of the thoracolumbar vertebrae in *Dasypsus* (Hautier et al., 2011; Fig. 6). While all early embryonic vertebrae display a rather simple and homogenous saddle shape (Hautier et al., 2018), they ossify at different times. The early embryonic peak in disparity might reflect this differential timing of ossification, an effect that might be mitigated later in development when all vertebrae are well ossified. The region-specific disparity analyses enabled us to look more closely at this pattern (Fig. 4B). We observed that the drop in disparity is found almost entirely in the anterior thoracic vertebrae, which suggests that vertebrae in this region display distinctive shapes early during development. Anatomical comparisons showed that the first two thoracics are linked to cervicals via the brachial plexus (Buchholtz et al., 2014; Alcântara et al., 2020). Several studies (e.g. Head and Polly, 2015; Jones et al., 2018b) also found that the first thoracic vertebra of *Mus musculus* is morphologically regionalised with the post-atlanto-axial cervical series, which was confirmed by our regionalisation analyses (specimen G, fig. 2A; specimen D, Fig. 2B). Such a definite grouping was, however, not predicted for *Dasypus*, as their cervical vertebrae are totally lacking the neural spines that are so prominent in thoracic vertebrae, including the most anterior ones. Alternatively, this disparity pattern might be attributable primarily to differences in ossification timing. Hautier et al., (2010) showed that the first two sets of thoracic neural arches ossify before their posterior neighbours in *D. novemcinctus* (Fig. 6B and C), so that their grouping in younger specimens could be due to a relatively more advanced development at this stage. Such an

explanation would account for the diminishing effect of this pattern through ontogeny, when the more posterior thoracic vertebrae start exhibiting more derived morphologies.

Alongside disparity, the whole-column integration was expected to increase across development, especially postnatally, as vertebral function and mobility are dependent on the individual units working in tandem. This trend was observed across our specimens, but there is a dramatic increase in juveniles and adults. The timing of this elevated integration corresponds with the development of the xenarthrous articulations and may facilitate interactions among these tightly interlocking joints. Previous studies (Bergmann et al., 2006; Jones and German, 2014) proposed that functional demands on the vertebral column differ prenatally, neonatally, and in adulthood. Naturally, neonates require integrated vertebral columns as much as juveniles and adults, but ranges of axial movements might be more limited at younger stages or be facilitated by cartilaginous units that could not be taken into account here. The consideration of such cartilaginous parts might have resulted in higher values of integration and disparity in early stages of development, thereby shifting the curve to the left (Fig. 4).

Rates of growth - Our findings also indicate that the regionalisation of the vertebral column may stem from different vertebral growth rates. Few data exist on the role of growth in the evolution of the axial regionalisation (Bergmann and Russell, 2001; Bergmann et al., 2003, 2004, 2006; Jones et al 2014). Bergmann et al. (2006) exhibited differential growth rates between vertebrae and vertebral regions in rats, with individual vertebrae showing increasing growth craniocaudally. Jones and German (2014) concurred with such a pattern of craniocaudally increasing growth and showed that growth of a particular vertebra is a function of its position within the vertebral column. However, all these previous attempts focused on the

development of the centrum, whose shape is more easily traceable using X ray radiography on longitudinal data. Our results based on neural arches showed rather contrasted results, with the neural arches of the xenarthrous thoracic region growing slowest, and the anterior thoracic and lumbar growing at increasing rates, craniad and caudad respectively. Such differences suggest that distinct developmental pathways contribute to axial skeleton regulation of the neural arches and centra, which was confirmed by previous analyses of modularity (e.g. Hautier et al., 2010; Randau and Goswami, 2017b).

In terms of function, slower growth rates in the middle of the dorsal column may reflect increasing relative stiffness in response to sagging forces that occur midway between the limbs (Smit, 2002). Moreover, some consistent patterns seem to emerge between differential growth rates and ossification timings. The vertebral region that displays the slowest growth rates corresponds to the last region to ossify its neural arches, which comprises the meeting point between an ossification that spreads caudally from the anterior thoracic region and another that spreads cranially from the lumbar region. Henry et al. (2007) showed that in naked mole rats different vertebral regions respond differently to systematic growth hormones to drive differentiation. We then argue that regional differences in the ossification sequence and growth patterns might be determined by regionalisation, which in turn shape morphology. The fact that thoracolumbar centra usually display an anteroposterior ossification sequence (Hautier et al., 2010, 2014) and a pattern of craniocaudally increasing growth (Bergmann et al., 2006; Jones and German, 2014) is in line with this proposition. However, these results have to be taken cautiously as growth rates might be variable through ontogeny. Differences might exist between prenatal and postnatal growth, with vertebrae showing slow prenatal growth but fast postnatal growth (Bergmann et al., 2006), or regions growing more quickly than others but for a shorter period of

time (Reichling and German, 2000). Our dataset prevents us from identifying specific bursts of growth through ontogeny or differences in growth rates between stages.

In the mouse, the delayed ossification region also matches with the posterior limit of HoxA4 and is near the anterior limit of HoxA9 expression (Hautier et al., 2014; Fig. 6), and Hautier et al. (2014) suggested that ossification may be another aspect of axial skeleton phenotype influenced by *Hox* regulation. Mutations in *Hox* complexes lead to modification in vertebra identity, as defined by vertebra shape and connectivity to ribs/girdles at the end of embryonic development in the mouse (Wellik and Capecchi, 2003). However, while *Hox* genes express very early during development, no *Hox* gene has yet been shown to directly affect vertebral growth rate or timing of ossification, and the direct effects of the *Hox* code on the later processes of vertebral development have yet been elucidated. In mouse and chick models, these later processes include the determination of ventral somite cells into sclerotome cells (Neubuser et al., 1995; Muller et al., 1996), the migration of sclerotome cells, condensation and differentiation of chondroblasts (Wallin et al., 1994; Peters et al., 1999; Makino et al., 2013), the chondrocyte differentiation and hypertrophy (Crean et al., 1997; Makino et al., 2013), and the endochondral and perichondral ossification through differentiation of osteoblasts from sclerotome cells and calcification (Hermann-Kleiter et al., 2009; Makino et al., 2013). All these events involve different sets of developmental genes. In essence, differential growth timings and rates might constitute an integral part of vertebral identity, and could be influenced by *Hox* genes or by their downstream patterning. However, several developmental factors such as mechanical loadings are also known to influence vertebral growth, and the duration and rate of growth of a particular vertebra might only reflect the pattern of growth of surrounding tissues (O'Higgins et al., 1997).

CONCLUSION

Here we applied a developmental perspective to the regionalisation of the axial skeleton of *D. novemcinctus* and showed that vertebrae adopt their unique morphology and become consistently regionalised early during development. Although vertebral morphologies transition gradually, the number of vertebral regions seems to be conserved during development despite drastic changes in morphology. The distinction between non-xenarthrous and xenarthrous vertebrae may constitute the more dominant shift, as demonstrated by our regionalisation and trajectory analyses, while the classic division of the trunk between thoracic and lumbar might represent a more secondary shift and relate more to ribs than vertebrae themselves. By tracing the development of vertebral morphologies from foetal to adult stages, we showed that vertebral morphotypes and axial modularity are likely influenced by variations in size, developmental tempo and growth rates. However, further comparisons, notably between the centra and the neural arches, are needed to understand how these growth patterns are genetically mediated.

Acknowlegments

We thank Judy Chupasko, Mark Omura and Mark Renczkowski [Museum of Comparative Zoology, Harvard University (MCZ)] for all of their help during the course of this project, Frank M. Knight (University of the Ozarks) and Benoit de Thoisy (Institut Pasteur, Cayenne, French Guiana) for donating armadillo carcasses, and several colleagues in the MCZ for helping with experimental setup and data collection (Robert Kambic, Brianna McHorse, Blake Dickson and Hanna Barnes). A version of this paper was submitted by J.D.O. in partial fulfilment of the Erasmus Mundus Master Programme in Evolutionary Biology.

Competing interests

The authors declare no competing or financial interests.

Author contributions

Concepts and approach were developed by J.D.O., L.H. and S.E.P. Experiments and data analysis was performed by J.D.O., L.H., K.E.J. and S.E.P. The manuscript was prepared by J.D.O. and L.H., and edited by K.E.J. and S.E.P. prior to submission.

Funding

This study was partially funded by National Science Foundation grant number EAR-1524523 to S.E.P., and through a Category A Erasmus Mundus scholarship (European Commission) to J.D.O.

REFERENCES

Adams, D. C., and M. L. Collyer. 2009. A general framework for the analysis of phenotypic trajectories in evolutionary studies. Evolution 63:1143–1154.

Adams, D. C., M. Collyer, and A. Kaliontzopoulou. 2020. geomorph: Geometric Morphometric Analyses of 2D/3D Landmark Data. Version 3.2.1. R Package.

Alcântara, S. F., M. J. A. L. Amorim, P. V. Albuquerque, E. P. Mesquita, M. E. L. C. Miranda, G. P. Andrade, N. E. O. Nascimento, and J. C. S. Nascimento. 2020. Description of brachial plexus of sloth (Bradypus variegatus). Pesquisa Veterinária Brasileira 40:824–829.

Anderson, G. E., and S. M. Secor. 2016. Differential growth of body segments explains

ontogenetic shifts in organ position for the Diamondback Water Snake (Nerodia rhombifer). Canadian Journal of Zoology 94:651–660.

Bateman, N. 1954. Bone growth: a study of the grey-lethal and microphthalmic mutants of the mouse. Journal of Anatomy 88:212–62.

Bergmann, P. J., A. D. Melin, and A. P. Russell. 2006. Differential segmental growth of the vertebral column of the rat (Rattus norvegicus). Zoology 109:54–65.

Boszczyk, B. M., A. A. Boszczyk, and R. Putz. 2001. Comparative and functional anatomy of the mammalian lumbar spine. Anatomical Record 264:157–168.

Buchholtz, E. A. 2001. Vertebral osteology and swimming style in living and fossil whales (Order: Cetacea). Journal of Zoology 253:175–190.

Buchholtz, E. A. 2007. Modular evolution of the Cetacean vertebral column. 289:278–289.

Buchholtz, E. A., K. L. Wayrynen, and I. W. Lin. 2014. Breaking constraint: Axial patterning in Trichechus (Mammalia: Sirenia). Evolution and Development 16:382–393.

Burke, A. C., C. E. Nelson, B. A. Morgan, and C. Tabin. 1995. Hox genes and the evolution of vertebrate axial morphology. Development 121:333–346.

Collyer, M. L., and D. C. Adams. 2013. Phenotypic trajectory analysis: Comparison of shape change patterns in evolution and ecology. Hystrix 24.

Crean, J., S. Roberts, D. Jaffray, S. Eisenstein, and V. Duance. 1997. Matrix Metalloproteinases in the Human Intervertebral Disc: Role in Disc Degeneration and Scoliosis. Spine 22:2877–2884.

Cubo, J., D. Azagra, A. Casinos, and J. Castanet. 2002. Heterochronic detection through a function for the ontogenetic variation of bone shape. Journal of Theoretical Biology 215:57–66.

Emerling, C., and M. Springer. 2015. Genomic evidence for rod monochromacy in sloths and armadillos suggests early subterranean history for Xenarthra. Proceedings of the Royal Society B 282:2014.2192.

Frechkop, S. 1949. Explication biologique, fournie par les tatous, d'un des caractères distinctifs des xénarthres et d'un caractère adaptif analogue chez les pangolins. Bulletin de l'Institut Royal Des Sciences Naturelles de Belgique 25:1–12.

Gal, J. M. 1993. Mammalian spinal biomechanics□: II. intervertebral lesion experiments and mechanisms of bending resistance. Journal of Experimental Biology 174:281–297.

Gál, J. M. 1993. Mammalian spinal biomechanics. I. Static and dynamic mechanical properties of intact intervertebral joints. Journal of Experimental Biology 174:247–280.

Gaudin, T. 1999. The morphology of xenarthrous vertebrae (Mammalia: Xenarthra). Field Museum of Natural History 41:1–52.

Gaudin, T., and A. Biewener. 1992. The functional morphology of xenarthrous vertebrae in the armadillo *Dasypus novemcinctus* (Mammalia, Xenarthra). Journal of Morphology 214:63–81.

Gómez-Robles, A., and P. D. Polly. 2012. Morphological integration in the hominin dentition: evolutionary, developmental, and functional factors. Evolution 66:1024–1043.

Hautier, L., J. D. Oliver, and S. E. Pierce. 2018. An Overview of Xenarthran Developmental Studies with a Focus on the Development of the Xenarthrous Vertebrae. Journal of Mammalian Evolution 25:507–523.

Hautier, L., C. Charles, R. J. Asher, and S. J. Gaunt. 2014. Ossification sequence and genetic patterning in the mouse axial skeleton. Journal of Experimental Zoology Part B: Molecular and Developmental Evolution.

Hautier, L., V. Weisbecker, M. R. Sánchez-Villagra, A. Goswami, and R. J. Asher. 2010. Skeletal development in sloths and the evolution of mammalian vertebral patterning. Proceedings of the National Academy of Sciences of the United States of America 107:18903–18908.

Hautier, L., V. Weisbecker, A. Goswami, F. Knight, N. Kardjilov, and R. J. Asher. 2011. Skeletal ossification and sequence heterochrony in xenarthran evolution. Evolution and Development 13:460–476.

Head, J. J., and P. D. Polly. 2015. Evolution of the snake body form reveals homoplasy in amniote Hox gene function. Nature 520:86–89.

Hebrank, J. H., M. R. Hebrank, J. H. Long, B. A. Block, and S. A. Wainwright. 1990. Backbone mechanics of the blue marlin Makaira nigricans (Pisces, Istiophoridae). Journal or Experimental Biology 148:449–459.

Henry, E. C., C. M. Dengler-crish, and K. C. Catania. 2007. Growing out of a caste – reproduction and the making of the queen mole-rat. Journal of Evolutionary Biology 210:261–268.

Hermann-Kleiter, N., N. Ghaffari-Tabrizi, M. J. F. Blumer, C. Schwarzer, M. A. Mazur, and I. Artner. 2009. Lasp1 misexpression influences chondrocyte differentiation in the vertebral column. International Journal of Developmental Biology 53:983–991.

Jenkins, F. 1970. Anatomy and function of expanded ribs in certain edentates and primates. Journal of Mammalogy 51:288–301.

Johnson, D. R., and P. O'Higgins. 1994. The inheritance of patterns of metameric variation in the mouse (Mus musculus) vertebral column. Journal of Zoology 233:473–492.

Jones, K. E., and R. Z. German. 2014. Ontogenetic allometry in the thoracolumbar spine of

mammal species with differing gait use. Evolution and Development 16:110–120.

Jones, K. E., L. Benitez, K. D. Angielczyk, and S. E. Pierce. 2018a. Adaptation and constraint in the evolution of the mammalian backbone. BMC Evolutionary Biology 18:33–35.

Jones, K. E., S. Gonzalez, K. D. Angielczyk, and S. E. Pierce. 2020. Regionalization of the axial skeleton predates functional adaptation in the forerunners of mammals. Nature Ecology and Evolution 4:470–478.

Jones, K. E., K. D. Angielczyk, P. D. Polly, J. J. Head, V. Fernandez, J. K. Lungmus, S. Tulga, and S. E. Pierce. 2018b. Fossils reveal the complex evolutionary history of the mammalian regionalized spine. Science 361:1249–1252.

Klingenberg, C. P. 2008. Novelty and "homology-free" morphometrics: What's in a name? Evolutionary Biology 35:186–190.

Koob, T. J., and J. H. Long. 2000. The vertebrate body axis: Evolution and mechanical function1. American Zoologist 40:1–18.

Lebrun, R. 2014. ISE-MeshTools software. http://morphomuseum. com/meshtools. Morphomuseum Journal.

Long, J. H., D. A. Pabst, W. R. Shepherd, and W. A. McLellan. 1997. Locomotor design of dolphin vertebral columns: bending mechanics and morphology of Delphinus delphis. Journal of Experimental Biology 200:65–81.

MacPhee, R. 1994. Morphology, adaptations, and relationships of *Plesiorycteropus*: and a diagnosis of a new order of eutherian mammals. Bulletin of the American Museum of Natural History 220:1–214.

Makino, Y., Y. Takahashi, R. Tanabe, Y. Tamamura, T. Watanabe, M. Haraikawa, M. Hamagaki, K. Hata, J. Kanno, T. Yoneda, Y. Saga, M. Goseki-Sone, K. Kaneko, A.

Yamaguchi, and T. Limura. 2013. Spatiotemporal disorder in the axial skeleton development of the Mesp2-null mouse: A model of spondylocostal dysostosis and spondylothoracic dysostosis. Bone 53:248–258.

Muller, T., C. Ebensperger, A. Neubuser, H. Koseki, R. Balling, B. Christ, and J. Wilting. 1996. Expression of avian Pax1 and Pax9 is intrinsically regulated in the pharyngeal endoderm, but depends on environmental influences in the para- xial mesoderm. Developmental Biology 178:403–417.

Neubuser, A., H. Koseki, and R. Balling. 1995. Characterization and developmental expression of Pax9, a paired-box-con- taining gene related to Pax1. Developmental Biology 170:701–716.

Nyakatura, J. A., and M. S. Fischer. 2011. Functional morphology of the muscular sling at the pectoral girdle in tree sloths: convergent morphological solutions to new functional demands? Journal of Anatomy 219:360–374.

O'Higgins, P., N. Milne, D. R. Johnson, C. K. Runnion, and C. E. Oxnard. 1997. Adaptation in the vertebral column: a comparative study of patterns of metameric variation in mice and men. Journal of Anatomy 190:105–113.

Oliver, J. D., K. E. Jones, L. Hautier, W. J. Loughry, and S. E. Pierce. 2016. Vertebral bending mechanics and xenarthrous morphology in the nine-banded armadillo (*Dasypus novemcinctus*). The Journal of Experimental Biology 219:2991–3002.

Olson, R. A., M. D. Womble, D. R. Thomas, Z. D. Glenn, and M. T. Butcher. 2016. Functional morphology of the forelimb of the nine-banded armadillo (Dasypus novemcinctus): comparative perspectives on the myology of Dasypodidae. Journal of Mammalian Evolution 23:49–69.

Peters, H., B. Wilm, N. Sakai, K. Imai, R. Maas, and R. Balling. 1999. Pax1 and Pax9 synergistically regulate vertebral column development. Development 126:5399–5408.

Pierce, S. E., J. A. Clack, and J. R. Hutchinson. 2011. Comparative axial morphology in pinnipeds and its correlation with aquatic locomotory behaviour. Journal of Anatomy 219:502–514.

Randau, M., and A. Goswami. 2017a. Morphological modularity in the vertebral column of Felidae (Mammalia, Carnivora). BMC Evolutionary Biology 17:1–12.

Randau, M., and A. Goswami. 2017b. Unravelling intravertebral integration, modularity and disparity in Felidae (Mammalia). Evolution and Development 19:85–95.

Randau, M., A. Goswami, J. R. Hutchinson, A. R. Cuff, and S. E. Pierce. 2016. Cryptic complexity in felid vertebral evolution: shape differentiation and allometry of the axial skeleton. Zoological Journal of the Linnean Society 178:183–202.

Reichling, T. D., and R. Z. German. 2000. Bones, muscles and visceral organs of protein-malnourished rats (Rattus norvegicus) grow more slowly but for longer durations to reach normal final size. The Journal of Nutrition 130:2326–2332.

Rockwell, H., F. G. Evans, and H. C. Pheasant. 1938. The comparative morphology of the vertebrate spinal column: its function as related to function. Journal of Morphology 63:87–117.

Schilling, N. 2011. Evolution of the axial system in craniates: Morphology and function of the perivertebral musculature. Frontiers in Zoology 8:1–19.

Simpson, G. 1931. Metacheiromys and the Edentata. Bulletin American Museum of Natural History 59:295–381.

Smith, S. M., and K. D. Angielczyk. 2020. Deciphering an extreme morphology: Bone

microarchitecture of the hero shrew backbone (Soricidae: Scutisorex). Proceedings of the Royal Society B: Biological Sciences 287.

Valverde, E., E. Gálvez-López, C. Alba-Fernández, L. Del Río, and A. Casinos. 2010. Lumbar ontogenetic growth and sexual dimorphism in modern humans. American Journal of Human Biology 22:596–603.

Vizcaino, S. F., and N. Milne. 2002. Structure and function in armadillo limbs (Mammalia□: Xenarthra□: Dasypodidae). Journal of Zoology 257:117–127.

Wallin, J., J. Wilting, H. Koseki, R. Fritsch, B. Christ, and R. Balling. 1994. The role of Pax-1 in axial skeleton development. Development 120:1109–1121.

Wellik, D., and M. Capecchi. 2003. How10 and Hox11 genes are required to globally pattern the mammalian skeleton. Science. 301:363–366.

Wellik, D. M. 2007. Hox Patterning of the Vertebrate Axial Skeleton. Developmental Dynamics 236:2454–2463.

Young, R. L., and A. V. Badyaev. 2006. Evolutionary persistence of phenotypic integration: influence of developmental and functional relationships on complex trait evolution. Evolution 60:1291.

Tables

Table 1 - Specimens included in analyses. Specimens are listed in order of assumed increasing age, and are provided with average centroid sizes of the left neural arch, and their assigned stages. Specimens were aged according to extent of vertebral ossification, as observed in reconstructions of microCT scans. Average centroid sizes of left neural arches generally agree with this ranking, with inconsistencies due to intraspecific variation.

Specimen ID	Museum ID	Average centroid size	Stage
A	ZMB 7b	2.95	Embryo
B	ZMB 40645	3.80	Embryo
C	ZMB 40648	3.75	Embryo
D	ZMB 40647	5.46	Embryo
E	ZMB 85979	4.56	Embryo
F	BMNH 2010_90_98_1	8.31	Embryo
G	USNM 254678	6.92	Neonate
H	USNM 204180	7.85	Neonate
I	USNM 2960	7.59	Neonate
J	USNM 21954	12.23	Neonate
K	UM-M1508	11.05	Juvenile
L	MCZ 67404	31.00	Juvenile
M	MCZ 67407	40.88	Adult
N	MCZ 67402	40.47	Adult
O	MCZ 67401	38.47	Adult

Table 2 - Locations of landmarks on the left neural arch.

Number	**Definition**
1	Dorsocranial corner of neural spine
2	Dorsocaudal corner of neural spine
3	Ventrocranial corner of neural arch
4	Ventrocaudal corner of neural arch
5	Ventrocranial point of fusion to centrum
6	Ventrocaudal point of fusion to centrum
7	Lateralmost point of metapophysis
8	Ventral base of metapophysis on neural arch
9	Dorsocaudal point of anapophysis
10	Caudal base of anapophysis on neural arch
11	Caudal extension of neural arch

12	Lateralmost point of diapophysis
13	Ventral base of diapophysis on neural arch
14	Lateral tip of postzygapophysis
15	Ventral base of postzygapophysis on neural arch
16	Cranialmost point of caudal concavity

Table 3 - Vertebral regions identified according to centroid shape and size. Regions identified according to shape are listed on the left, and regions identified according to size are on the right. Region score refers to the weighted mean derived from AIC analyses of regionalisation, which is rounded to identify the number of regions in the best model. Break points identify the locations within the thoracolumbar region separating the regions. Break point vertebrae are included in the anterior region, e.g. the three regions identified in Specimen A span from thoracic vertebrae (T) one to five, thoracics six to nine, and thoracic ten to lumbar (L) five.

	Shape			Size		
Specimen	Region score	Regions	Break point(s)	Region score	Regions	Break point(s)
A	3.00	3	T5, T9	2.12	2	T7
B	2.15	2	T6	2.00	2	T5
C	2.86	3	T3, T7	2.00	2	T5
D	2.96	3	T3, T8	2.91	3	T2, T6
E	3.00	3	T5, T10	2.03	2	T6
F	2.20	2	T6	2.00	2	T4
G	3.83	4	T2, T6, T10	2.21	2	T6
H	2.94	3	T5, T10	2.00	2	T6
I	3.00	3	T5, T10	2.01	2	T6
J	2.98	3	T5, T8	2.01	2	T5
K	2.72	3	T5, T8	2.09	2	T6
L	3.00	3	T5, T10	2.00	2	T7
M	3.00	3	T6, T10	2.05	2	T5
N	3.00	3	T6, T10	2.00	2	T7
O	3.00	3	T6, T10	2.00	2	T6

Table 4 – Pairwise comparisons between phenotypic trajectories of the vertebral regions between developmental stages. Significant differences and *p*-values according to $p \leq 0.05$ are bolded.

	Size *P* value	Direction *P* value	Shape *P* value
Embryo x Neonate	**0.004**	**0.001**	0.873
Embryo x Juvenile	**0.001**	**0.001**	0.565
Embryo x Adult	**0.001**	**0.001**	0.081
Neonate x Juvenile	**0.001**	**0.001**	0.625
Neonate x Adult	**0.001**	**0.001**	0.157
Juvenile x Adult	**0.041**	0.118	0.518

Table 5 - Pairwise comparisons between phenotypic trajectories of the developmental stages between vertebral regions. Significant differences and *p*-values according to $p \leq 0.05$ are bolded.

	Size *P* value	Direction *P* value	Shape *P* value
Ta x Tx	**0.001**	**0.001**	0.054
Ta x L	**0.002**	**0.001**	0.181
Tx x L	0.143	**0.001**	0.847

Table 6 - Pairwise differences of regional morphological disparities across developmental stages. Absolute pairwise difference between disparities are presented in the top right of each region, and *p*-values of the corresponding comparisons are presented in the bottom left. Significant differences and *p*-values according to $p \leq 0.05$ are bolded.

		Embryo	Neonate	Juvenile	Adult
			Ta		
Ta	Embryo	/	0.0260	**0.0554**	**0.1749**
	Neonate	0.1717	/	**0.0814**	**0.2009**
	Juvenile	**0.0206**	**0.0012**	/	**0.1196**
	Adult	**0.0001**	**0.0001**	**0.0001**	/
			Tx		

Tx	Embryo	/	0.0037	0.019	**0.0525**
	Neonate	0.8699	/	0.0227	**0.0562**
	Juvenile	0.5261	0.4946	/	0.0335
	Adult	**0.0398**	**0.0388**	0.307	/
			L		
L	Embryo	/	0.0013	**0.0855**	**0.1683**
	Neonate	0.952	/	**0.0868**	**0.1696**
	Juvenile	**0.0018**	**0.0021**	/	**0.0823**
	Adult	**0.0001**	**0.0001**	**0.0053**	/

Figure captions

Figure 1 – Landmarks digitized on the vertebrae. Lateral (A), anterior (B), and posterior (C) views. *Abbreviations*: ap, anapophysis; ax, anterior xenarthrous facet; mp, metapophysis; ns, neural spine; pmz, posterior medial zyg-apophysis; vc, vertebral centrum.

Figure 2 - Vertebral regions predicted by (A) shape and (B) size, as identified according to the data presented in Table 2. Vertebral identities are denoted on the bottom of the figure, ranging from thoracic one (T1) to lumbar five (L5).

Figure 3 - (A) Vertebral morphospace as identified by a principal component analysis. Symbol shapes characterize vertebral regions: squares are anterior thoracics, diamonds are xenarthrous thoracics, and triangles are lumbars. (B) Phenotypic trajectories are drawn between vertebral regions within each developmental stage. Symbol colors and shapes follow (A). Small coloured symbols denote individual vertebrae, and large coloured symbols denote the means of each vertebral region within each stage. The large white circles represent the means of anterior thoracic vertebrae in each stage, and the large black circles represent the means of lumbar vertebrae. (C) Phenotypic trajectories are drawn for each region across development. Symbol shapes follow (A). As in (B), small coloured symbols denote individual vertebrae, and large coloured symbols denote regional means within each developmental stage, with the exception of the large white symbols, which represent the mean of juvenile specimens, and the large black symbols which represent the mean of adult specimens.

Figure 4 - Morphological disparity and integration across development. In (A), whole-column disparity and integration are plotted across individuals, in order from youngest to oldest. In (B), regional disparity is plotted across the four developmental stages.

Figure 5 – (A) Proportion of each vertebra, as compared to size of the thoracolumbar region during the four developmental stages (i.e embryos, neonates, juveniles, and adults) (B) Regression slopes plotted for the centroid of each vertebral position against the size of the thoracolumbar region for all individuals. The slope is then used as an estimator of vertebral growth.

Figure 6 - Summary of ossification sequences in the long-nosed armadillo (*Dasypus*) vertebral elements. Hox expression boundaries in the mouse (redrawn from Meyer and Gruss, 1993; Gaunt *et al*., 1988, 1999) and vertebral segment identity are shown at left. Dorsal view of the rib cage in wild type mice (A) and three fetuses of armadillo (B, C, and D). Vertebral neural arches are in red, vertebral centra are in blue, scapula and clavicle are in green, and ischium, ilium, and pubis are in orange. For clarity, elements of the zeugopod have been removed.

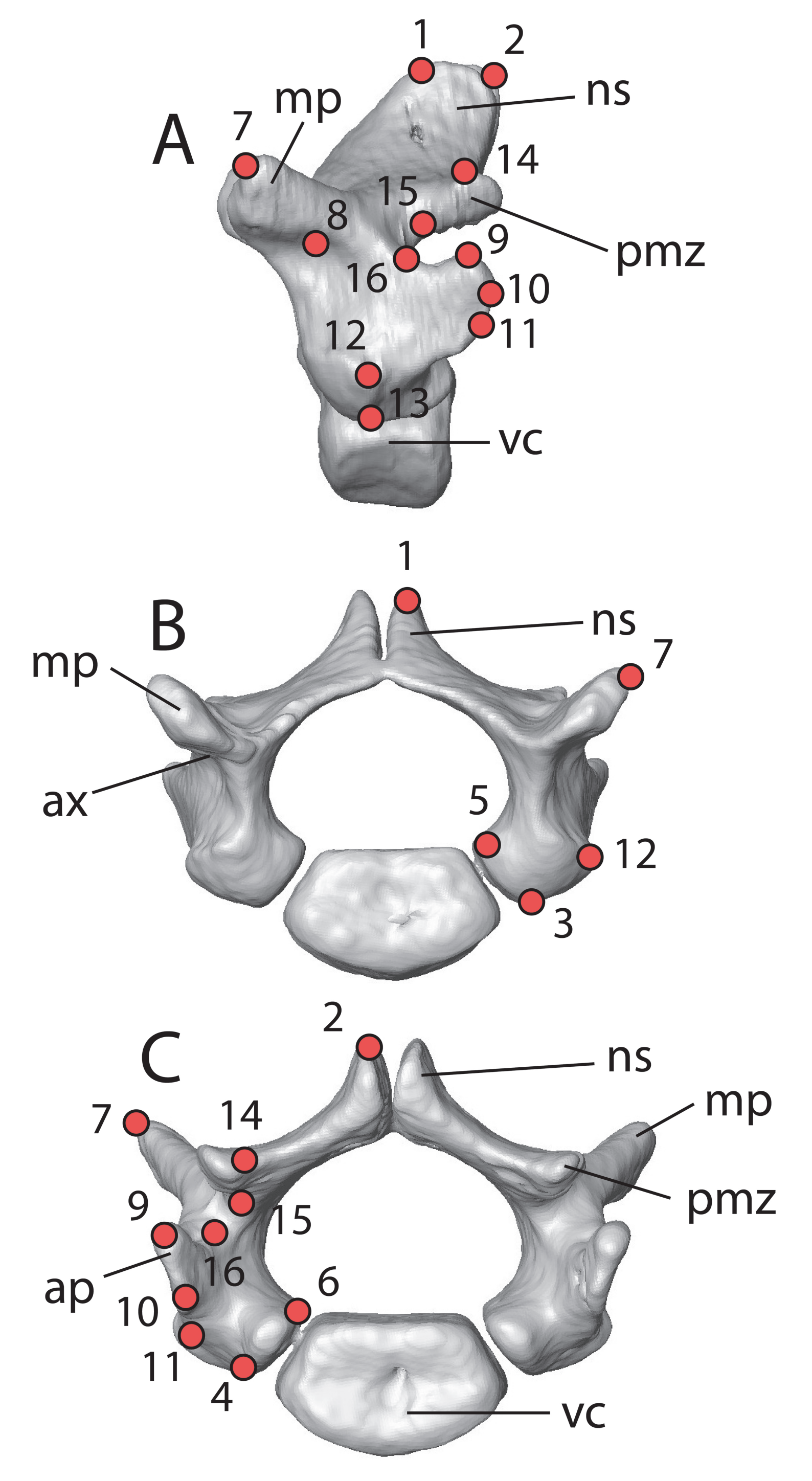
A
1
2
ns
mp
7
14
15
8
9
pmz
16
10
12
11
13
vc
B
1
ns
mp
7
ax
5
12
3
C
2
ns
7
14
mp
9
15
pmz
ap
16
6
10
11
4
vc

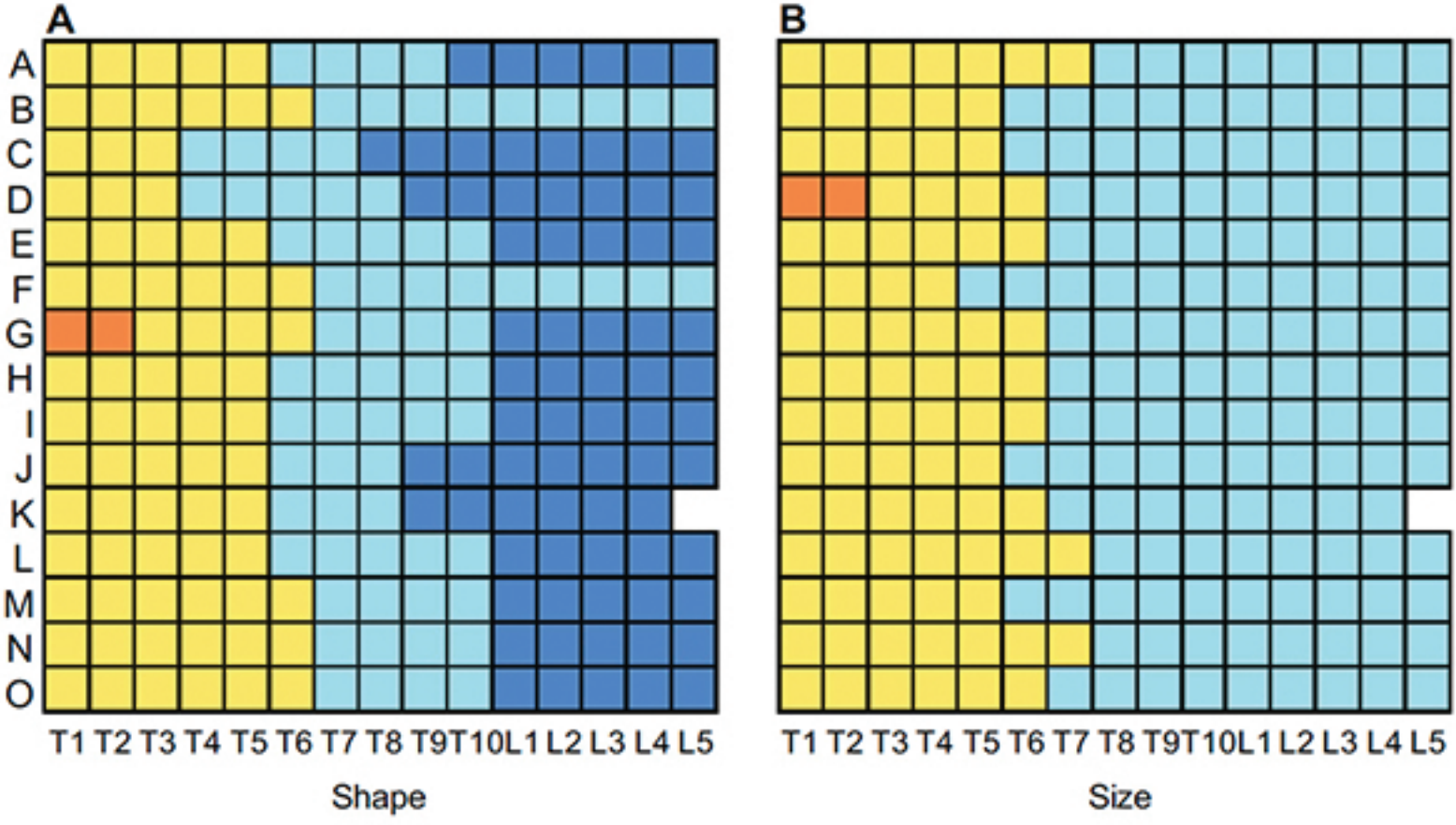
A
B
A
B
C
D
E
F
G
H
I
J
K
L
M
N
O
T1 T2 T3 T4 T5 T6 T7 T8 T9 T10 L1 L2 L3 L4 L5
Shape
T1 T2 T3 T4 T5 T6 T7 T8 T9 T10 L1 L2 L3 L4 L5
Size

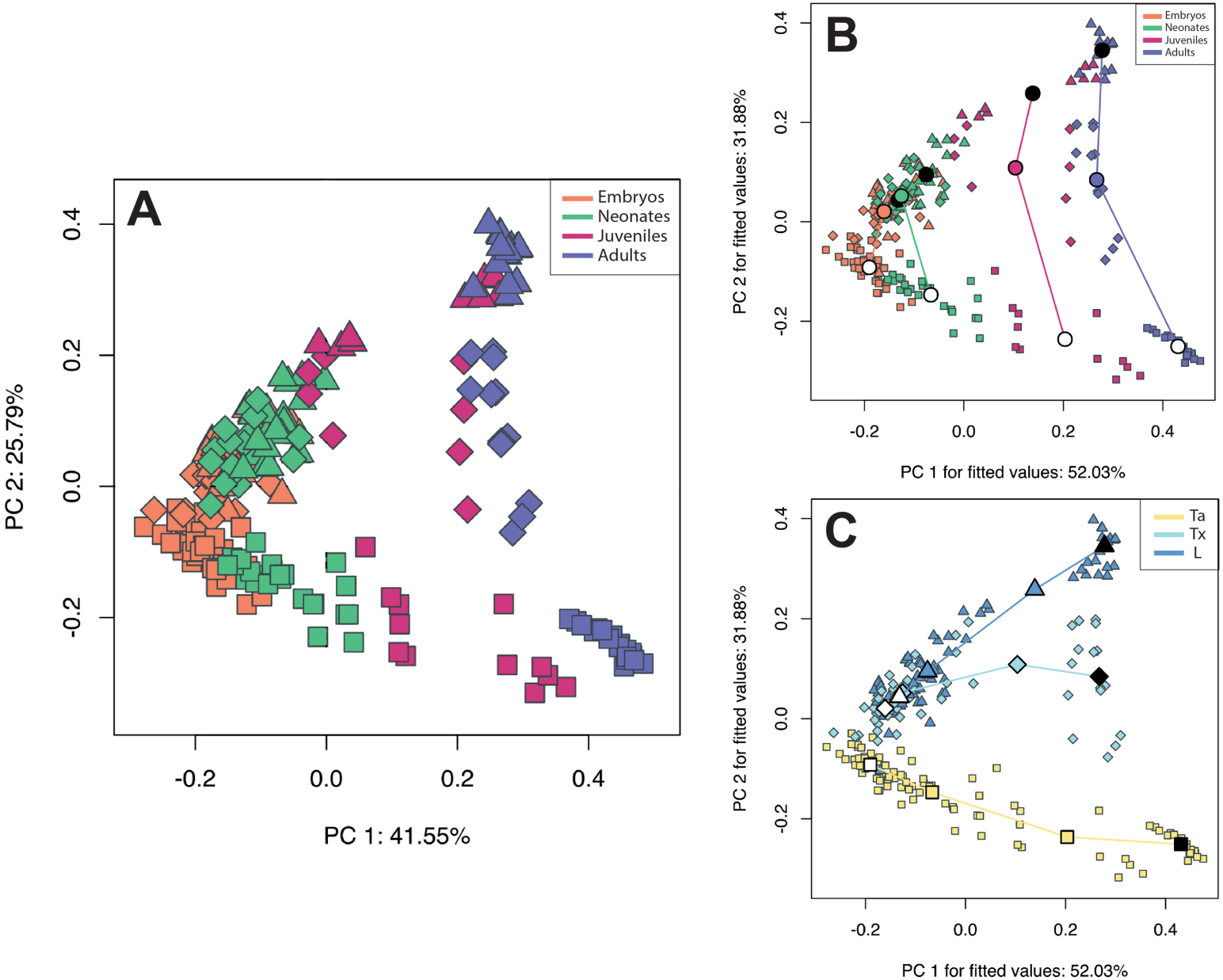
A
Embryos
Neonates
Juveniles
Adults
PC 2: 25.79%
PC 1: 41.55%
B
Embryos
Neonates
Juveniles
Adults
PC 2 for fitted values: 31.88%
PC 1 for fitted values: 52.03%
C
Ta
Tx
L
PC 2 for fitted values: 31.88%
PC 1 for fitted values: 52.03%

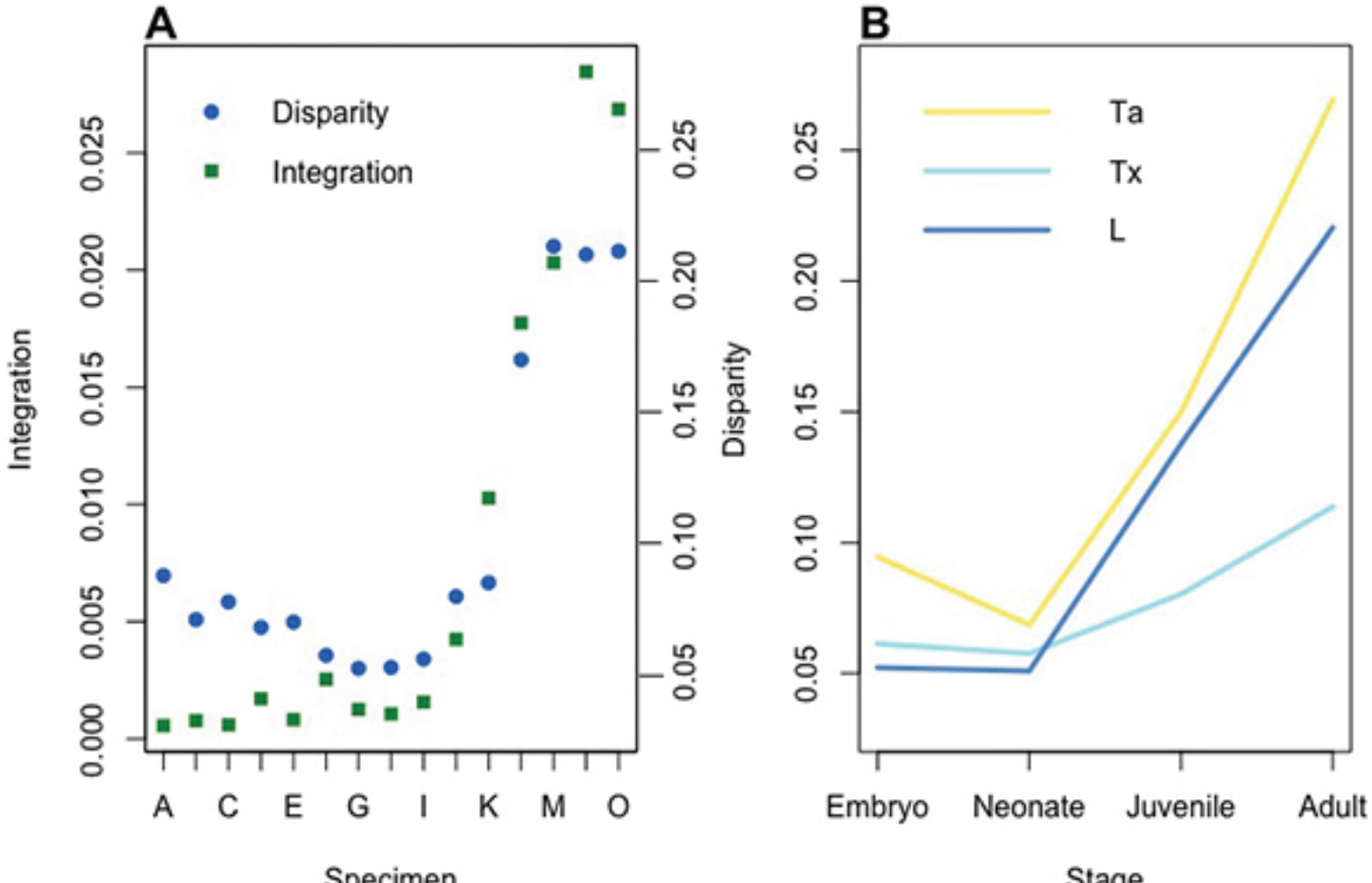
A
Disparity
Integration
Integration
0.000
0.005
0.010
0.015
0.020
0.025
Disparity
0.05
0.10
0.15
0.20
0.25
A
C
E
G
I
K
M
O
Specimen
B
Ta
Tx
L
0.05
0.10
0.15
0.20
0.25
Embryo
Neonate
Juvenile
Adult
Stage

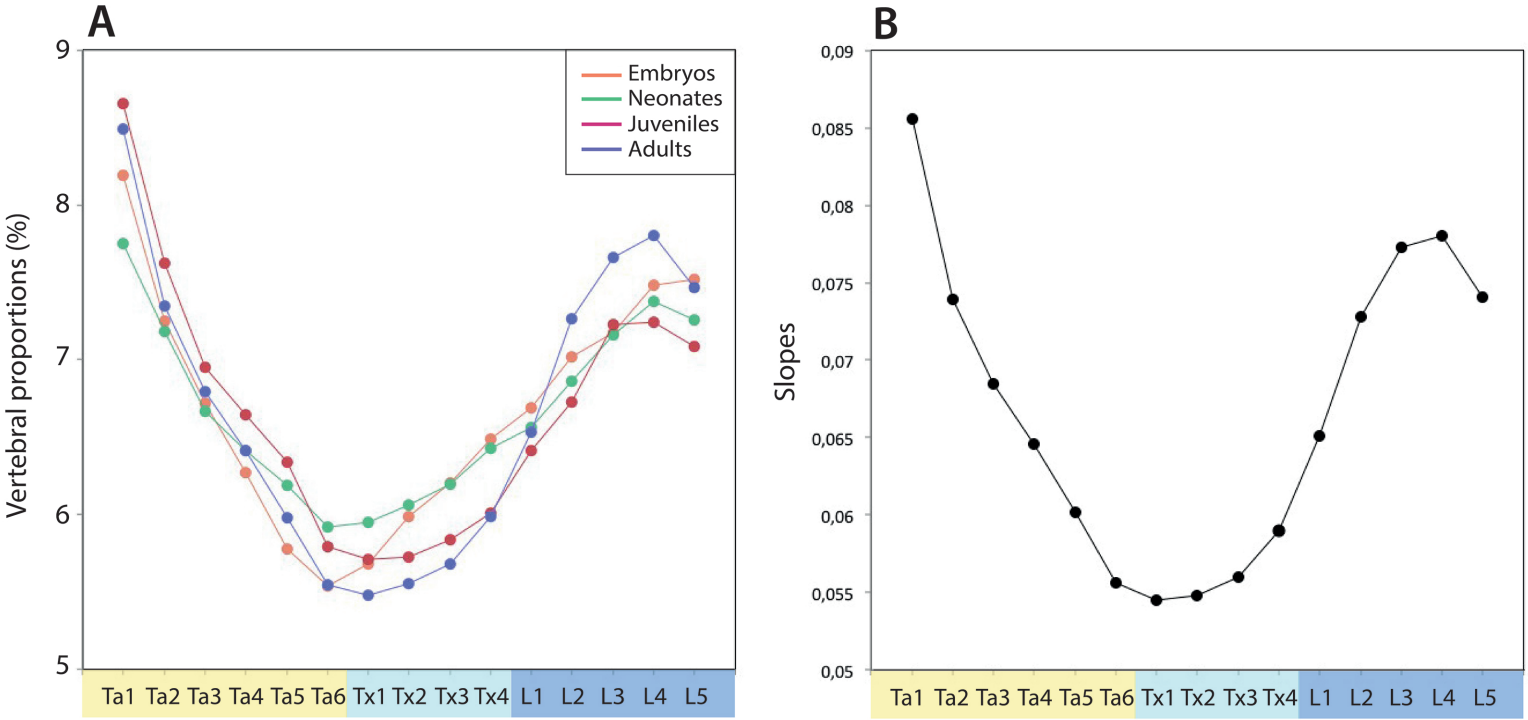
A
Vertebral proportions (%)
9
8
7
6
5
Embryos
Neonates
Juveniles
Adults
Ta1 Ta2 Ta3 Ta4 Ta5 Ta6 Tx1 Tx2 Tx3 Tx4 L1 L2 L3 L4 L5
B
Slopes
0,09
0,085
0,08
0,075
0,07
0,065
0,06
0,055
0,05
Ta1 Ta2 Ta3 Ta4 Ta5 Ta6 Tx1 Tx2 Tx3 Tx4 L1 L2 L3 L4 L5

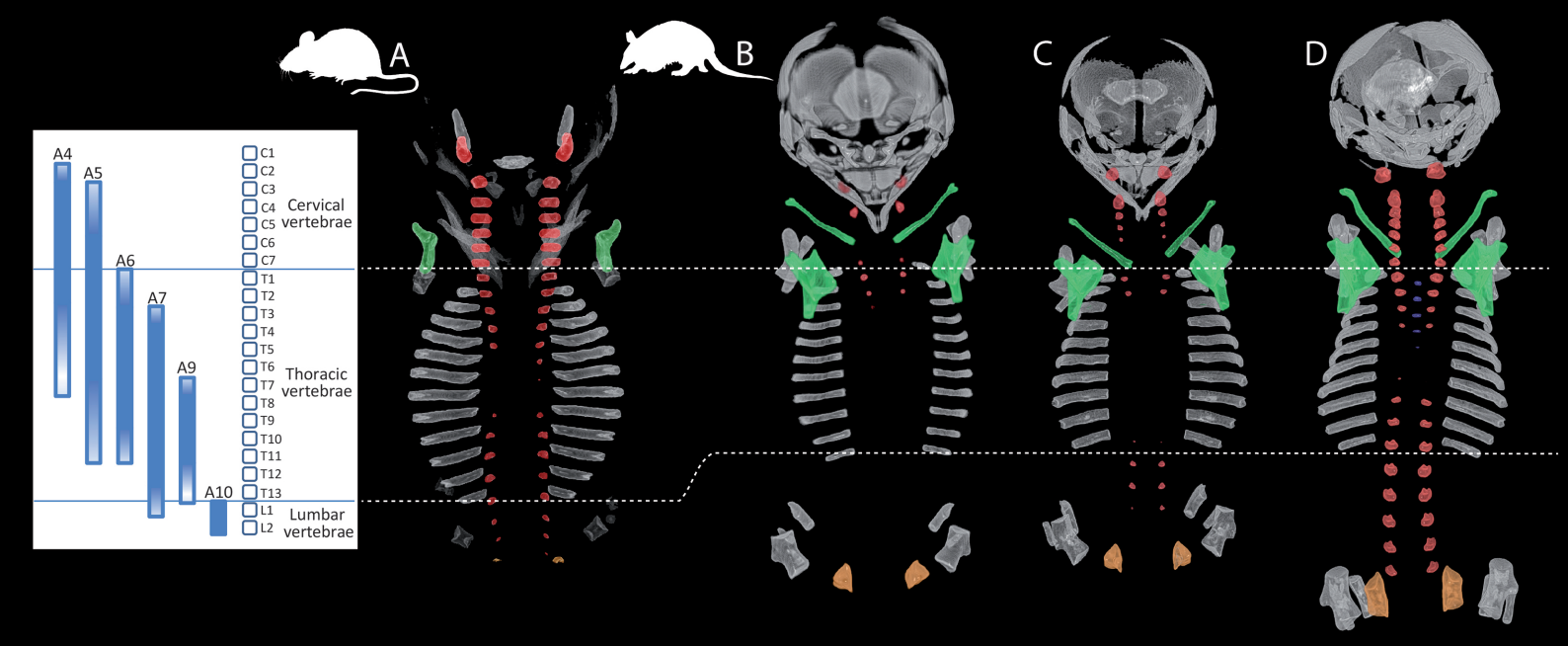
A
B
C
D
A4
A5
A6
A7
A9
A10
C1
C2
C3
C4
C5
C6
C7
T1
T2
T3
T4
T5
T6
T7
T8
T9
T10
T11
T12
T13
L1
L2
Cervical vertebrae
Thoracic vertebrae
Lumbar vertebrae